

## Giant voltage modulation of magnetic anisotropy in strained heavy metal/magnet/insulator heterostructures

P. V. Ong,<sup>1</sup> Nicholas Kioussis,<sup>1,\*</sup> D. Odkhuu,<sup>1</sup> P. Khalili Amiri,<sup>2</sup> K. L. Wang,<sup>2</sup> and Gregory P. Carman<sup>3</sup>

<sup>1</sup>*Department of Physics and Astronomy, California State University Northridge, Northridge, California 91330, USA*

<sup>2</sup>*Department of Electrical Engineering, University of California, Los Angeles, California 90095, USA*

<sup>3</sup>*Department of Mechanical and Aerospace Engineering, University of California, Los Angeles, California 90095, USA*

(Received 21 December 2014; revised manuscript received 12 April 2015; published 20 July 2015)

*Ab initio* electronic structure calculations reveal that epitaxial strain has a dramatic effect on the voltage-controlled magnetic anisotropy (VCMA) in Ta/FeCo/MgO junctions. Strain can give rise to a wide range of novel VCMA behaviors where the MA can change from a  $\nabla$ - to a  $\wedge$ -shape electric-field dependence with *giant* VCMA coefficients which are asymmetric under voltage reversal. The underlying mechanism is the interplay of the strain- and electric-field-induced changes in the spin-orbit coupled  $d$  states at the interfaces and the strain-induced modification of the dielectric constant of MgO. These findings demonstrate the feasibility of highly sensitive VCMA through strain engineering, which may provide a viable avenue for tailoring magnetoelectric properties for spintronic applications.

DOI: [10.1103/PhysRevB.92.020407](https://doi.org/10.1103/PhysRevB.92.020407)

PACS number(s): 75.85.+t, 73.20.-r, 75.30.Gw, 75.70.Cn

Even though the switching of magnetization in magnetic random access memory (RAM) bits using spin-polarized currents via the spin transfer torque (STT) effect has proven very successful [1], it requires high current densities and hence high power consumption. Furthermore, the switching energy per bit ( $\sim 100$  fJ) of STT-RAM is still around two orders of magnitude higher compared with complementary metal-oxide semiconductor switching energies of  $\sim 1$  fJ [2]. A highly promising approach for developing ultralow power, highly scalable, and nonvolatile spin-based RAMs is the voltage-controlled magnetic anisotropy (VCMA) of heavy metal/ferromagnet/insulator (HM/FM/I) nanojunctions via the magnetoelectric effect (MeRAM) [3–6] where the nonmagnetic HM contact electrode (Ta, Pd, Pt, and Au) has strong spin-orbit coupling (SOC). In the low-bias regime the VCMA is proportional to the electric field ( $E$  field) in the insulator,  $VCMA = \beta E_l = \beta \frac{E_{ext}}{\epsilon}$ , where  $\beta$  is the VCMA coefficient,  $\epsilon$  is the dielectric constant of the I, and  $E_{ext}$  is the external  $E$  field. The challenge for achieving a switching bit energy below 1 fJ and a write voltage below 1 V requires large perpendicular MA (PMA) [4,7] and  $\beta \geq 200$  fJ  $V^{-1} m^{-1}$  [2].

The VCMA of HM/FM/I junctions exhibits a wide range of behavior ranging from linear with positive or negative  $\beta$  to nonmonotonic  $\nabla$ -shape or inverse- $\nabla$ - ( $\wedge$ -) shape  $E$ -field dependence with asymmetric  $\beta$ 's. On the experimental side, a linear VCMA was observed in epitaxial Au/FeCo/MgO [8] and in Ta/Co<sub>40</sub>Fe<sub>40</sub>B<sub>20</sub>/MgO [9] tunnel junctions with  $\beta$  of  $-38$  and  $-33$  fJ  $V^{-1} m^{-1}$ , respectively, where the convention of the positive  $E$  field corresponds to the accumulation of electrons in the FM/I interface. On the other hand, a  $\nabla$ -shape VCMA was found in Au/Fe/MgO [5]. Furthermore, in Ta/Co<sub>40</sub>Fe<sub>40</sub>B<sub>20</sub>/MgO/Co<sub>40</sub>Fe<sub>40</sub>B<sub>20</sub> junctions the coercivity of the bottom FM electrode decreases linearly with voltage with  $\beta \approx 50$  fJ  $V^{-1} m^{-1}$  whereas that of the top FM electrode exhibits a  $\nabla$ -shape voltage behavior [6].

Recent experiments in Pd/FePd/MgO [10], V/Fe/MgO [11], and MgO/FeB/MgO/Fe [12] junctions show linear  $\wedge$ - and  $\nabla$ -shape VCMA with giant  $\beta$  values of about 600, 1150, and 100 fJ  $V^{-1} m^{-1}$ , respectively. Although in general the underlying mechanism remains unresolved, a possible origin of the nonmonotonic VCMA in V/Fe/MgO may be due to the internal  $E$  field caused by charges trapped by defects in MgO [11]. On the theoretical side, *ab initio* electronic structure calculations of Fe/MgO [13] and Au/Fe/MgO [14] junctions with in-plane lattice constants of Fe and MgO, respectively, predicted a linear VCMA with  $\beta$  of about  $+130$  and  $+70$  fJ  $V^{-1} m^{-1}$ , respectively.

The fairly large lattice mismatch (4% to 5%) among the I, the FM, and the HM layers in these heterostructures invites several intriguing and important questions which remain unexplored. What is the effect of strain on the: (1) the VCMA behavior and its coefficients, (2) the dielectric constant and hence the  $E_l$ , and (3) the critical field where the MA reaches its maximum or minimum value? The purpose of this Rapid Communication is to employ *ab initio* electronic structure calculations to understand the effect of epitaxial strain on the VCMA behavior of the Ta/FeCo/MgO junction and reconcile the origin of the experimental controversies. We demonstrate that the strain can selectively tune the VCMA from the  $\nabla$  to  $\wedge$  shape with *giant* VCMA coefficients which are asymmetric upon  $E$ -field switching.

The *ab initio* electronic structure calculations have been carried out within the framework of the projector augmented-wave formalism [15] as implemented in the Vienna *ab initio* simulation package (VASP) [16,17] with the generalized gradient approximation [18] for the exchange-correlation functional. The slab supercell for the Ta/FeCo/MgO (001) junction along [001] consists of three monolayers (MLs) of bcc Ta on top of three MLs of  $B2$ -type FeCo on top of seven MLs of rock-salt MgO and a 15-Å-thick vacuum region. The O atoms at the FeCo/MgO interface are placed atop Fe atoms. We denote with Fe1 and Fe2 [the inset in Fig. 1(a)] the atoms at the Fe/MgO and Fe/Ta interfaces, respectively. The expansive strain  $\eta_{FeCo}$  on the FeCo film is varied from

\*nick.kioussis@csun.edu

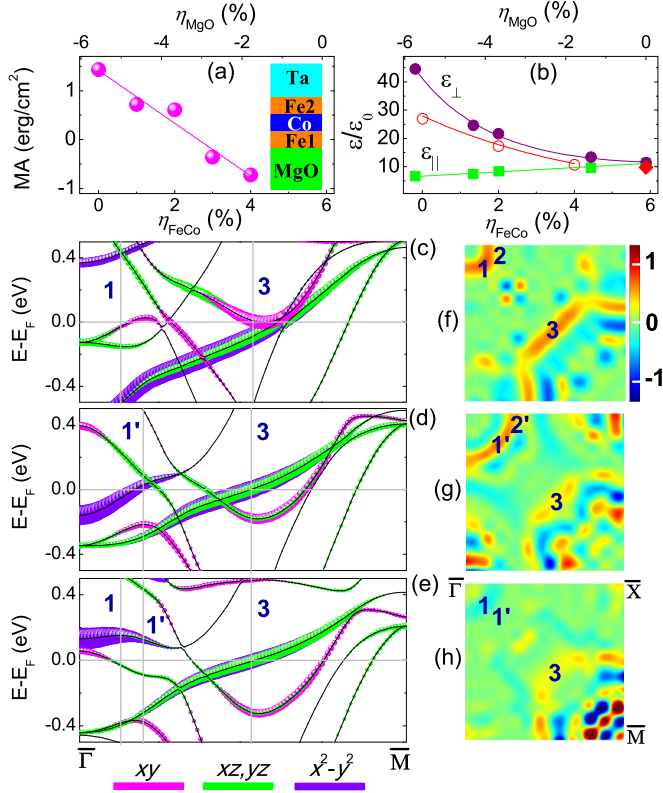


FIG. 1. (Color online) (a) Strain dependence of zero-field MA of the Ta/FeCo/MgO junction where the expansive (compressive) strain  $\eta_{\text{FeCo}}$  ( $\eta_{\text{MgO}}$ ) is shown along the bottom (top) ordinate. (b) Strain dependence of the relative in-plane (solid squares) and out-of-plane (solid circles) components ( $\epsilon_{\parallel}$  and  $\epsilon_{\perp}$ ) of the dielectric tensor of bulk MgO and of  $\epsilon_{\perp}$  for the MgO thin film (open circles). (c)–(e) Energy- and  $k$ -resolved distributions of the orbital character of minority-spin bands along  $\Gamma\bar{M}$  for the interfacial Fe1 atom  $d$  states for  $\eta_{\text{FeCo}} = 0\%$ ,  $2\%$ , and  $4\%$ , respectively. (f)–(h) MA( $\mathbf{k}$ ) (in meV) in the two-dimensional (2D) Brillouin zone (BZ) for  $\eta_{\text{FeCo}} = 0\%$ ,  $2\%$ , and  $4\%$ , respectively. Numerals in panels (c)–(h) refer to BZ  $\mathbf{k}$  points (BZP $n$ ,  $n = 1$ –3) where there are large changes in MA.

0% to 4% to simulate the effect of in-plane strain under experimental conditions [19]. At each strain, the magnetic and electronic degrees of freedom and atomic positions along [001] are relaxed in the presence of the  $E$  field. Employing a  $31 \times 31 \times 1$   $k$ -point mesh, the MA per unit interfacial area  $A$  is determined from  $\text{MA} = [E_{[100]} - E_{[001]}]/A$ , where  $E_{[100]}$  and  $E_{[001]}$  are the total energies with magnetization along the [100] and [001] directions, respectively.

*Effect of strain on zero-field MA.* Figure 1(a) shows the strain dependence of the zero-field MA of the Ta/FeCo/MgO junction. We find that the MA decreases almost linearly with increasing strain and undergoes a transition from an out-of-plane to an in-plane magnetization at  $\sim \eta_{\text{FeCo}} = +2.5\%$ . From the strain dependence of the MA (see the Supplemental Material [20]) we find that the effective interfacial uniaxial magnetocrystalline anisotropy  $K_2^i = 1.41$  erg/cm<sup>2</sup> and the interfacial magnetoelastic coefficient  $B_1^i = -18.81$  erg/cm<sup>2</sup>.

Furthermore, epitaxial strain has a large effect on the dielectric constant of MgO which in turn controls the magnitude of  $E_I$  at the FM/I interface. Employing density-functional

calculations as implemented in the PWSCF package [21], we display in Fig. 1(b) the out-of-plane ( $\epsilon_{\perp}$ ) and in-plane ( $\epsilon_{\parallel}$ ) components of the relative dielectric tensor of bulk MgO versus in-plane strain. We find that  $\epsilon_{\perp}$  increases exponentially from its zero-strain value of 9.8 with increasing compressive  $\eta_{\text{MgO}}$  strain indicating a decrease in  $E_I$ . This result is further corroborated by independent VASP slab calculations for the Ta/FeCo/MgO junction, where  $\epsilon_{\perp}$  (open circles) is determined from the ratio of the  $E$  field in vacuum to that in MgO where the latter is determined from the change in the planar average electrostatic potential.

To elucidate the mechanism of the strain effect on the zero-field MA, we show in Figs. 1(c)–(e) the energy- and  $k$ -resolved distribution of the minority-spin band of the Fe1-derived  $d_{xy}$ ,  $d_{xz/yz}$ , and  $d_{x^2-y^2}$  states along the  $\Gamma\bar{M}$  symmetry direction for  $\eta_{\text{FeCo}} = 0\%$ ,  $2\%$ , and  $4\%$ , respectively. We find that the strain-induced change in the zero-field MA arises primarily from changes in the band structure of the Fe1 interfacial atom. We have employed both the total energy method and the force theorem [22]  $\text{MA} = \sum_{\mathbf{k}} \text{MA}(\mathbf{k})$  to calculate the effect of strain on the MA. The  $k$ -resolved  $\text{MA}(\mathbf{k}) \approx \sum_{n \in \text{occ}} [\epsilon(n, \mathbf{k})^{[100]} - \epsilon(n, \mathbf{k})^{[001]}]$  in the 2D BZ is shown in Figs. 1(f)–(h) for  $\eta_{\text{FeCo}} = 0\%$ ,  $2\%$ , and  $4\%$ , respectively. Here,  $\epsilon(n, \mathbf{k})^{[100]([001])}$  are the eigenvalues of the Hamiltonian for magnetization along the [100] ([001]) direction. Using the force theorem we find that  $\text{MA} = 1.98$ ,  $0.69$ , and  $-0.83$  erg/cm<sup>2</sup> for  $\eta_{\text{FeCo}} = 0\%$ ,  $2\%$ , and  $4\%$ , respectively. These values agree well with those obtained from total energy calculations of  $1.43$ ,  $0.61$ , and  $-0.83$  erg/cm<sup>2</sup> for the corresponding strain values. Within second-order perturbation theory the MA can be expressed as [23]

$$\text{MA} \propto \xi^2 \sum_{o,u} \frac{|\langle \Psi_o^{\downarrow} | \hat{L}_z | \Psi_u^{\downarrow} \rangle|^2 - |\langle \Psi_o^{\downarrow} | \hat{L}_x | \Psi_u^{\downarrow} \rangle|^2}{E_u^{\downarrow} - E_o^{\downarrow}}, \quad (1)$$

where  $\Psi_o^{\downarrow}$  ( $E_o^{\downarrow}$ ) and  $\Psi_u^{\downarrow}$  ( $E_u^{\downarrow}$ ) are the one-electron occupied and unoccupied minority-spin states (energies) of band index  $n$  and wave vector  $\mathbf{k}$  (omitted for simplicity),  $\xi$  is the SOC, and  $\hat{L}_{x(z)}$  is the  $x$  ( $z$ ) component of the orbital angular momentum operator. This expression is valid when the majority band is full and the SOC between states of opposite spin can be ignored. Analysis of the density of states and the energy- and  $k$ -resolved distribution of  $d$  orbitals shows that the majority-spin states of the interfacial Fe1 and Fe2 atoms are well below 0.5 eV from the Fermi level. Therefore, the spin-flip contribution is negligible. In the analysis below the wave functions are projected on the  $d$  orbitals.

At zero strain, the maxima of  $\text{MA}(k_{\parallel})$  in Fig. 1(f) occur around  $\bar{\Gamma}$  along the  $\bar{\Gamma}\bar{M}$  (BZP1) and  $\bar{\Gamma}\bar{X}$  (BZP2) directions and around  $\frac{1}{2}\bar{\Gamma}\bar{M}$  (BZP3). The underlying origin of the MA maxima at BZP1 and BZP2 is the SOC between the minority-spin interfacial Fe1-derived occupied  $d_{xy}$  and  $d_{xz(yz)}$  states with the unoccupied  $d_{x^2-y^2}$  and  $d_{yz(xz)}$  states, respectively, in Fig. 1(c), through the  $\hat{L}_z$  operator. On the other hand, the MA maximum at BZP3 is due to the large SOC  $\langle x^2 - y^2 | \hat{L}_z | xy \rangle$  and  $\langle xz(yz) | \hat{L}_z | yz(xz) \rangle$  of Fe1.

Overall, an increase in strain induces large downward shifts of the minority-spin bands of the Fe1-derived  $d_{xy}$  and  $d_{xz(yz)}$  states and upward energy shifts of the  $d_{x^2-y^2}$  bands along

the  $\overline{\Gamma\text{M}}$  direction. This leads to substantial rearrangement of occupied and unoccupied bands and hence large changes in the matrix elements of the  $\hat{L}_z$  and  $\hat{L}_x$  operators throughout the 2D BZ. Thus, at 2% strain the SOC  $\langle x^2 - y^2 | \hat{L}_x | yz(xz) \rangle$  at BZP1 becomes dominant rendering the  $k$ -resolved MA(BZP1)  $< 0$  [blue ring around  $\overline{\Gamma}$  in Fig. 1(g)]. Furthermore, the increase in energy splitting between the occupied  $d_{xy}$ -derived and unoccupied  $d_{x^2-y^2}$ -derived bands as well as between the occupied  $d_{xz(yz)}$ -derived and unoccupied  $d_{yz(xz)}$ -derived bands at BZP3 leads to a decrease in the  $k$ -resolved MA(BZP3). Note, that under 2% strain the rearrangement of bands shifts the MA maximum from BZP1 to BZP1' due to large SOC  $\langle xy | \hat{L}_z | x^2 - y^2 \rangle$  [Fig. 1(g)]. Under 4% strain, the Fe1  $d_{xy}$  shifts further down in energy [Fig. 1(e)] leading to a reduction in MA at BZP1' and BZP3. The Fe1 SOC  $\langle yz(xz) | \hat{L}_x | x^2 - y^2 \rangle$  around  $\overline{\Gamma}$  becomes dominant resulting in the out-of-plane to in-plane magnetization transition.

**Effect of strain on VCMA.** The variation in the MA as a function of the E field in MgO is shown in Figs. 2(a)–2(c) for  $\eta_{\text{FeCo}} = 0\%$ , 2%, and 4%, respectively. The results reveal that strain can have a dramatic effect on the VCMA, which changes from: (i) a  $\nabla$  shape at zero strain with giant  $\beta$  values of  $-648$  (486)  $\text{fJ V}^{-1} \text{m}^{-1}$  for a negative (positive) E field, to (ii) a symmetric  $\wedge$  shape at 2% strain with  $\beta$  values of  $+252$  ( $-241$ )  $\text{fJ V}^{-1} \text{m}^{-1}$  for a negative (positive) E field, and to (iii) an asymmetric  $\wedge$  shape at 4% strain with  $\beta$  values of  $+189$  ( $-238$ )  $\text{fJ V}^{-1} \text{m}^{-1}$ . Note that at 4% the MA reaches its maximum value at  $E_I = 0.93$  V/nm, which is close to the breakdown voltage of the MgO film ( $\sim 1$  V/nm). Consequently, the experimentally measured VCMA appears linear. The underlying origin presumably arises from the fact that the *interface* bands depend on the magnetization direction due to the Rashba effect. The Rashba coupling, which is proportional to the *net* electric field  $E_z$  at the interface, has contributions from both the internal and the external fields

[24]. The critical field where the MA reaches its maximum or minimum value depends on the interplay between the two E fields where the internal E field can be tuned via strain. Interestingly, recent experiments have reported the influence of the internal E field at the FM/I interface on the voltage-dependent tunneling anisotropic magnetoresistance [25].

These VCMA coefficient values are the highest reported today and are larger by about an order of magnitude compared to most experimental values, except for those reported in Refs. [10,11] where charged defects may play a role. Furthermore, our predicted  $\beta$ 's are close to or larger than the value of  $\sim 200$   $\text{fJ V}^{-1} \text{m}^{-1}$  required to achieve a switching bit energy below 1 fJ in the next-generation MeRAMs. Thus, our results demonstrate that the VCMA and its coefficients can be selectively tuned via proper epitaxial strain engineering. The even dependence of the MA on the E field is not only of potential interest for MeRAM, but also for STT-RAM with PMA, where a  $\wedge$ -shaped VCMA can symmetrically reduce the switching current in both directions.

Figures 2(d)–2(f) show the difference between the out-of-plane and in-plane orbital moments  $\Delta m_o = m_o^{1001} - m_o^{100}$  for the Fe1 and Fe2 interfacial atoms as a function of the E field for  $\eta_{\text{FeCo}} = 0\%$ , 2%, and 4%, respectively. The E-field variation in  $\Delta m_o$  for the Co and Ta1 atoms is not shown because it is much weaker. For single atomic species FMs with large exchange splitting the MA is related to the orbital moment anisotropy via the Bruno expression  $\text{MA} = \xi \Delta m_o / (4\mu_B)$  [26]. This expression needs to be modified for structures consisting of multiple atomic species with strong hybridization [27]. Nevertheless, overall the results show that the E-field dependence of  $\Delta m_o$  for Fe2 (and to a lesser degree for Fe1) correlates well with that of the MA for all strain values. Furthermore,  $\Delta m_o > 0$  for Fe1 whereas  $\Delta m_o < 0$  for the Fe2 atom (except for  $E > 0$  at 4%), indicating that the Fe2/Ta interface favors in-plane MA in agreement with experiment [28]. This is due to the fact that, in contrast to Fe1, the Fe2-derived  $d_{x^2-y^2}$  density of states around the Fermi energy is low leading to a decrease in  $\langle xy | \hat{L}_z | x^2 - y^2 \rangle$ . Consequently, the SOC between the occupied  $d_{xy}$ -derived and the unoccupied  $d_{xz(yz)}$ -derived Fe2 states through  $\hat{L}_x$  becomes dominant.

In order to understand the VCMA behavior under zero strain we show in Fig. 3(a) the field-induced  $\Delta \text{MA}(\mathbf{k}) = \text{MA}(\mathbf{k}, E) - \text{MA}(\mathbf{k}, E = 0)$  along symmetry directions under  $E_I = \pm 0.37$  V/nm. We also show in Figs. 3(b) and 3(c), the shift in the zero-field minority-spin band structures (dotted curves) under fields of  $-0.37$  V/nm (green curves) and  $+0.37$  V/nm (red curves), respectively. The E-field-induced  $\Delta \text{MA}(\mathbf{k})$  in the 2D BZ is displayed in Figs. 3(d) and 3(e) for fields of  $-0.37$  and  $+0.37$  V/nm, respectively. Integration of the  $\Delta \text{MA}(\mathbf{k})$  over the 2D BZ for negative and positive fields yields induced MA values consistent with the  $\nabla$  shape of the VCMA at zero strain in Fig. 2(a). Since  $\Delta \text{MA} > 0$  the analysis below is focused on the positive peaks in Fig. 3(a). The  $\Delta \text{MA}(\mathbf{k}) > 0$  under  $E_I < 0$  in the vicinity of  $\overline{\Gamma}$  (peaks 1 and 2) is due to the downward energy shift in the unoccupied Fe1  $d_{x^2-y^2}$ -derived bands in contrast to the occupied Fe1  $d_{xy}$ -derived bands which remain unshifted. The coupling of these states via  $\hat{L}_z$  and the decrease in the denominator in Eq. (1) result in  $\Delta \text{MA}(\mathbf{k}) > 0$ . Around  $\frac{1}{3}\overline{\Gamma\text{M}}$  the negative field

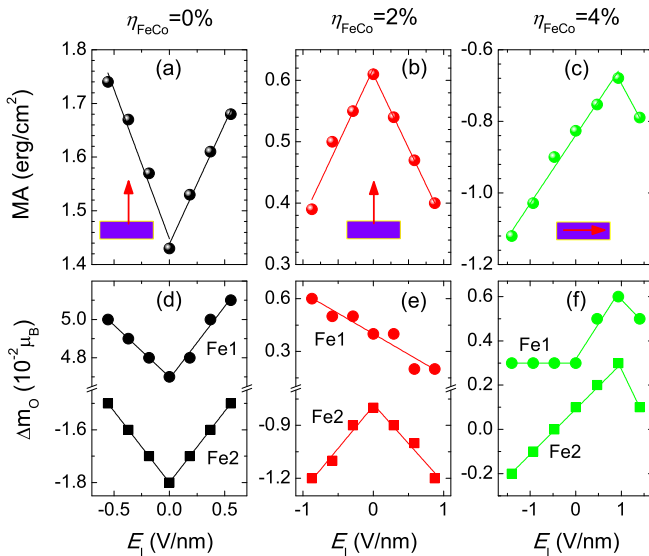


FIG. 2. (Color online) (a)–(c) MA versus E field in MgO for different strain values. (d)–(f) Orbital moment difference  $\Delta m_o = m_o^{1001} - m_o^{100}$  of the Fe1 and Fe2 interfacial atoms versus the E field for the same strain values.



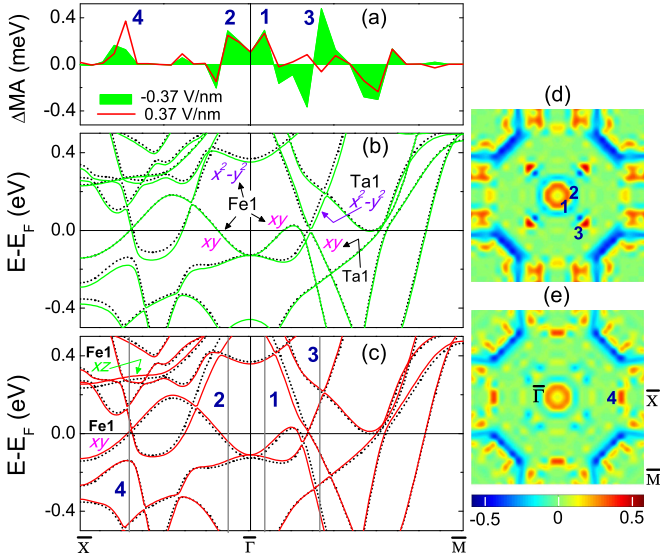


FIG. 3. (Color online) Zero strain: (a) E-field-induced  $\Delta MA(\mathbf{k})$  along symmetry directions for  $E_l = \pm 0.37$  V/nm. (b) and (c) Shift in zero-field minority-spin band structures (dotted curves) under  $-0.37$  V/nm (solid green curves) and  $+0.37$  V/nm (solid red curves) fields, respectively. We show the dominant Fe1 and Ta  $d$ -derived states. E-field-induced  $\Delta MA(\mathbf{k})$  (in meV) in the 2D BZ for (d)  $-0.37$  V/nm and (e)  $+0.37$  V/nm, respectively. The numbered vertical lines in (b) and (c) correspond to the numbered peaks in (a), (d), and (e).

has a negligible effect on the Ta1 occupied  $d_{xy}$ -derived states whereas it induces a significant shift in the Ta1 unoccupied  $d_{x^2-y^2}$ -derived states coupled via  $\hat{L}_z$ , resulting in  $\Delta MA(\mathbf{k}) > 0$  (peak 3).

Under  $+0.37$  V/nm both the Ta1 occupied  $d_{xy}$ -derived and the Ta1 unoccupied  $d_{x^2-y^2}$ -derived bands around  $\frac{1}{3}\bar{\Gamma}\bar{M}$  do not shift [Fig. 3(c)], and hence  $\Delta MA(\mathbf{k}) \rightarrow 0$  [Fig. 3(a)]. On the other hand, a new peak in  $\Delta MA(\mathbf{k})$  develops around  $\frac{2}{3}\bar{\Gamma}\bar{X}$  [peak 4 in Figs. 3(a) and 3(e)] due to the fact that both Fe1 occupied  $d_{xy}$ -derived and unoccupied  $d_{xz}$ -derived bands (coupled through  $\hat{L}_x$ ) shift up in energy rendering the  $d_{xy}$  states partially unoccupied. Thus, the out-of-plane contribution to  $MA(\mathbf{k})$  is enhanced.

At  $\eta_{\text{FeCo}} = 2\%$  the E-field-induced  $\Delta MA(\mathbf{k})$  is plotted along the high-symmetry directions in Fig. 4(a) for  $E_l = \pm 0.58$  V/nm. The shift in the zero-field minority-spin bands (dotted curves) are shown in Figs. 4(b) and 4(c) for an E field of  $-0.58$  V/nm (green curves) and  $+0.58$  V (red curves), respectively. Figures 4(d) and 4(e) display  $\Delta MA(\mathbf{k})$  in the 2D BZ for fields of  $-0.58$  V/nm and (e)  $+0.58$  V/nm,

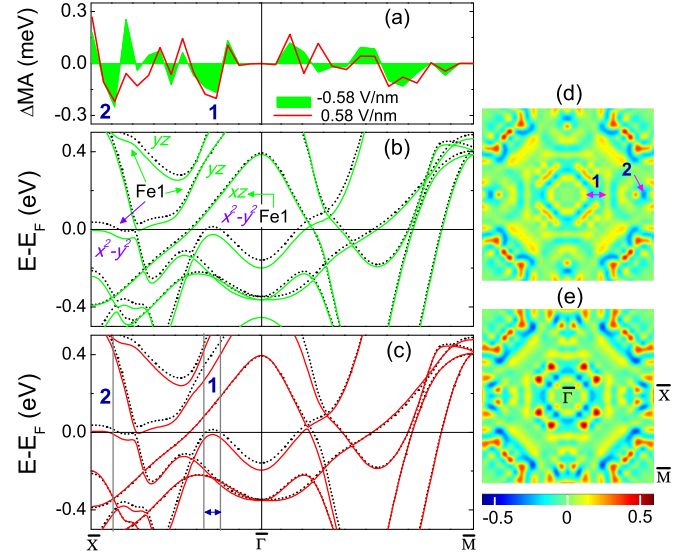


FIG. 4. (Color online) The same as Figs. 3(a)–3(e) but for 2% strain and  $E_l = \pm 0.58$  V/nm. We show only the dominant Fe1  $d$ -derived states in (b) and (c).

respectively. Integration of  $\Delta MA(\mathbf{k})$  over the 2D BZ for negative and positive fields yields induced MA values consistent with the  $\wedge$  shape of the VCMA at 2% strain in Fig. 2(b). Since for both field directions  $\Delta MA < 0$ , we focus on the main negative  $\Delta MA(\mathbf{k})$  troughs (1 and 2) in Figs. 4(a), 4(d), and 4(e) around  $\frac{1}{3}\bar{\Gamma}\bar{X}$  and near  $\bar{X}$ . Their origin lies on the field-induced shift in the Fe1  $d_{x^2-y^2}$ -derived bands from above to below the Fermi level [Figs. 4(b) and 4(c)] and the concomitant SOC of these states with the unoccupied Fe1  $d_{xz,yz}$  bands via  $\hat{L}_x$ , resulting in  $\Delta MA < 0$ .

To summarize, we have demonstrated that epitaxial strain, which is ubiquitous in many HM/FM/I trilayers, has a dramatic effect on the VCMA. It can change the VCMA from a  $\vee$ -shape to a  $\wedge$ -shape E-field dependence with *giant* VCMA coefficients. Furthermore, the critical field where the MA reaches its maximum or minimum value can be controlled selectively via strain tuning. These findings, which are general for other HM/FM/I junctions with different HM caps [29], open interesting prospects for exploiting strain engineering to harvest higher efficiency VCMA for the next generation MeRAM devices.

This research was supported by NSF under Grant No. 1160504 NSF Nanosystems Engineering Research Center (ERC) for Translational Applications of Nanoscale Multiferroic Systems (TANMS).

- [1] C. Chappert, A. Fert, and F. N. Van Dau, *Nature Mater.* **6**, 813 (2007).
- [2] K. L. Wang, J. G. Alzate, and P. Khalili Amiri, *J. Phys. D: Appl. Phys.* **46**, 074003 (2013).
- [3] Y. Shiota, T. Nozaki, F. Bonell, S. Murakami, T. Shinjo, and Y. Suzuki, *Nature Mater.* **11**, 39 (2012).

- [4] Y. Shiota, T. Maruyama, T. Nozaki, T. Shinjo, M. Shiraishi, and Y. Suzuki, *Appl. Phys. Express* **2**, 063001 (2009).
- [5] T. Maruyama, Y. Shiota, T. Nozaki, K. Ohta, N. Toda, M. Mizuguchi, A. A. Tulapurkar, T. Shinjo, M. Shiraishi, S. Mizukami, Y. Ando, and Y. Suzuki, *Nat. Nanotechnol.* **4**, 158 (2009).

- [6] W.-G. Wang, M. Li, S. Hageman, and C. L. Chien, *Nature Mater.* **11**, 64 (2012).
- [7] S. Ikeda, K. Miura, H. Yamamoto, K. Mizunuma, H. D. Gan, M. Endo, S. Kanai, J. Hayakawa, F. Matsukura, and H. Ohno, *Nature Mater.* **9**, 721 (2010).
- [8] T. Nozaki, Y. Shiota, M. Shiraishi, T. Shinjo, and Y. Suzuki, *Appl. Phys. Lett.* **96**, 022506 (2010).
- [9] M. Endo, S. Kanai, S. Ikeda, F. Matsukura, and H. Ohno, *Appl. Phys. Lett.* **96**, 212503 (2010).
- [10] F. Bonell, S. Murakami, Y. Shiota, T. Nozaki, T. Shinjo, and Y. Suzuki, *Appl. Phys. Lett.* **98**, 232510 (2011).
- [11] A. Rajanikanth, T. Hauet, F. Montaigne, S. Mangin, and S. Andrieu, *Appl. Phys. Lett.* **103**, 062402 (2013).
- [12] T. Nozaki, K. Yakushiji, S. Tamaru, M. Sekine, R. Matsumoto, M. Konoto, H. Kubota, A. Fukushima, and S. Yuasa, *Appl. Phys. Express* **6**, 073005 (2013).
- [13] M. K. Niranjan, C.-G. Duan, S. S. Jaswal, and E. Y. Tsymbal, *Appl. Phys. Lett.* **96**, 222504 (2010).
- [14] K. Nakamura, T. Akiyama, T. Ito, M. Weinert, and A. J. Freeman, *Phys. Rev. B* **81**, 220409(R) (2010).
- [15] P. E. Blöchl, *Phys. Rev. B* **50**, 17953 (1994).
- [16] G. Kresse and J. Furthmüller, *Phys. Rev. B* **54**, 11169 (1996).
- [17] G. Kresse and J. Furthmüller, *Comput. Mater. Sci.* **6**, 15 (1996).
- [18] J. P. Perdew, J. A. Chevary, S. H. Vosko, K. A. Jackson, M. R. Pederson, D. J. Singh, and C. Fiolhais, *Phys. Rev. B* **46**, 6671 (1992).
- [19] S. Yuasa, T. Nagahama, A. Fukushima, Y. Suzuki, and K. Ando, *Nature Mater.* **3**, 868 (2004).
- [20] See Supplemental Material at <http://link.aps.org/supplemental/10.1103/PhysRevB.92.020407> for the calculations of the magnetoelastic coefficients of the FM and the dielectric constant of the MgO layer.
- [21] S. Baroni, A. Dal Corso, S. de Gironcoli, and P. Giannozzi, <http://www.pwscf.org/>.
- [22] M. Weinert, R. E. Watson, and J. W. Davenport, *Phys. Rev. B* **32**, 2115 (1985).
- [23] D.-S. Wang, R. Wu, and A. J. Freeman, *Phys. Rev. B* **47**, 14932 (1993).
- [24] S. E. Barnes, J. Ieda, and S. Maekawa, *Sci. Rep.* **4**, 4105 (2014).
- [25] T. Uemura, M. Harada, K. Matsuda, and M. Yamamoto, *Appl. Phys. Lett.* **96**, 252106 (2010).
- [26] D. Weller, Y. Wu, J. Stöhr, M. G. Samant, B. D. Hermsmeier, and C. Chappert, *Phys. Rev. B* **49**, 12888 (1994).
- [27] C. Andersson, B. Sanyal, O. Eriksson, L. Nordström, O. Karis, D. Arvanitis, T. Konishi, E. Holub-Krappe, and J. Hunter Dunn, *Phys. Rev. Lett.* **99**, 177207 (2007).
- [28] H. Yamamoto, J. Hayakawa, K. Miura, K. Ito, H. Matsuoka, S. Ikeda, and H. Ohno, *Appl. Phys. Express* **5**, 053002 (2012).
- [29] P. V. Ong and N. Kioussis (unpublished).